Successive Self-Interference Cancellation in a Low-Complexity WCP-OFDM Radar Receiver

Steven Mercier, Damien Roque, Stéphanie Bidon

Successive Self-Interference Cancellation in a Low-Complexity WCP-OFDM Radar Receiver

Steven Mercier, Damien Roque and Stéphanie Bidon
Institut Supérieur de l'Aéronautique et de l'Espace (ISAE-SUPAERO), Université de Toulouse, 31055 Toulouse, FRANCE
Telephone: +33 5 61 33 87 53 Fax: +33 5 61 33 83 51
Email: {steven.mercier,damien.roque,stephanie.bidon}@isae-supaero.fr

***Abstract*—In this paper, we consider a multicarrier waveform to perform simultaneously data transmission and radar sensing. On the radar receiver side, a state-of-the-art symbol-based algorithm generates a range-Doppler map affected by a self-interference phenomenon, potentially leading to target masking issues. Herein, we propose a successive interference cancellation procedure to enhance the radar performance while keeping a low-complexity implementation. We show that a very low reconstruction error is obtained in various scenarios. We also investigate the robustness of the proposed algorithm since it is subject to error propagation.**

I. Introduction

As part of spectrum sharing techniques, waveform sharing between radar and communications systems may help to deal with the spectrum congestion problem. Besides radiofrequency's, it might as well save other types of resources such as energy, weight or volume and thereby address typical integration issues encountered in intelligent transportation systems, unmanned aerial vehicles, etc.

In this work, we focus on the radar processing applied to a multicarrier communication signal referred to as weighted cyclic prefix orthogonal frequency-division multiplexing (WCP-OFDM). The monostatic scenario we consider (also known as RadCom [1], see Fig. 1) allows the use of a 3-stage low-complexity radar architecture based on the knowledge of the transmitted symbols at the receiver [1], [2].

However, in practice, this approach was shown to result in a twofold self-interference phenomenon in the range-Doppler map [3], namely losses on the target peaks that translate into an increased white interference-plus-noise level, so that target masking is more likely to occur [4]. To address this issue while maintaining a low-computational complexity processing at the receiver, we here propose a Successive (self-) Interference Cancellation (SIC) algorithm inspired from the *ad-hoc* CLEAN procedure [5], [6].

The remaining of the paper is organized as follows. In Section II, expressions of the WCP-OFDM radar model and self-interference statistics are recalled to justify the need for mitigating this phenomenon. Section III exhibits the performance of our CLEAN-based SIC procedure assessed in both single and multitarget scenarios, as well as a robustness analysis. Finally, Section IV concludes and provides prospects for future work.

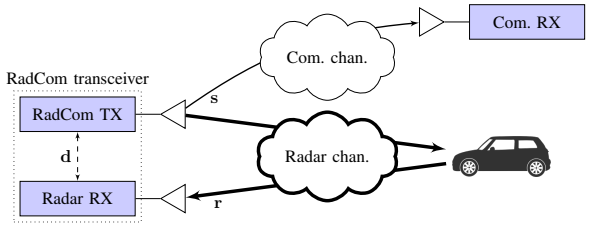

Fig. 1. Typical RadCom scenario involving a shared waveform to simultaneously perform monostatic radar sensing and data transmission.

II. RadCom system model

Herein, we recall the model of the low-complexity WCP-OFDM radar transceiver of [2], [3] and justify the need for mitigating the self-interference.

A. Waveform properties

The WCP-OFDM waveform is a generalization of the widespread cyclic prefix (CP-)OFDM to non-rectangular pulse-shapes that still implies: (i) transmit and receive pulses g and $\check{g}$ shorter than the duration of a multicarrier symbol, or block; (ii) perfect reconstruction (PR) of the data symbols on an ideal channel. Specifically in this paper, two types of WCP-OFDM pulse-shapes are focused on:

- the conventional rectangular pulses with CP;
- the time-frequency localized (TFL) pulses [7];

For radar sensing, the orthogonal scheme (*i.e.*, $\check{g} = g$) and improved frequency localization of TFL-pulses make them outperform CP-pulses in low-range and high-velocity scenarios [2], [3].

B. RadCom model

In the following, $\mathcal{I}_N$ stands for the finite set of integers $\{0, \dots, N-1\}$.

1) RadCom TX: The WCP-OFDM transmitter operates over K subcarriers along M blocks (or sweeps) to transmit a sequence of data symbols $\{d_{k,m}\}_{(k,m)\in\mathcal{I}_K\times\mathcal{I}_M}$. The latter are assumed to be independent and uniformly distributed in a constellation that is centrally symmetric, such as usual phase shift keying (PSK) or quadrature-amplitude modulation (QAM) constellations. The baseband transmitted signal sampled at critical rate $1/T_s$ can be expressed by blocks [8], [9]:

$$\mathbf{s} = \left[\mathbf{I}_M \otimes (\mathbf{D}_{\mathbf{g}}\mathbf{P}\mathbf{F}_K^H)\right]\mathbf{d} \tag{1}$$

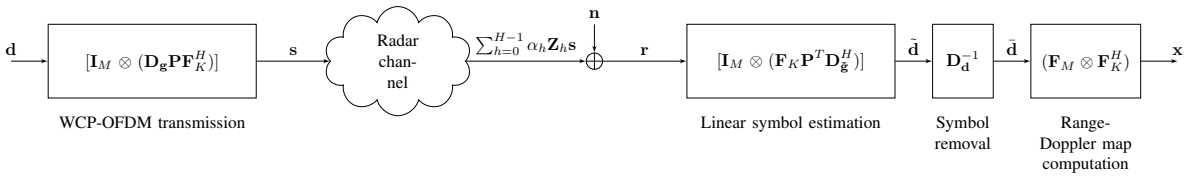

Fig. 2. Flowchart of the low-complexity WCP-OFDM radar transceiver.

where $\mathbf{d}$ is the symbol vector such that $[\mathbf{d}]_{k+mK} \triangleq d_{k,m}$, $\mathbf{F}_K$ the unitary K-DFT matrix, $\mathbf{P}$ the $L \times K$ cyclic extension matrix with expansion factor $L/K \geq 1$ involving the Kronecker symbol, namely $[\mathbf{P}]_{l,k} = \delta_{l,k} + \delta_{l,k+K}$, $\mathbf{D_g} = \mathrm{diag}(\mathbf{g})$ with $\mathbf{g} = [g[0], \ldots, g[L-1]]^T$ the transmit pulse-shape vector with ℓ_2-squared norm $\|\mathbf{g}\|^2 = K$, and $\mathbf{I}_M$ is the M-size identity matrix.

2) Radar channel: Consider H single-point targets with complex amplitudes α_h, round-trip delays $\tau_{0,h}$ and radial velocities v_h that partly backscatter the WCP-OFDM signal (1) towards the monostatic radar transceiver. Particularly, we assume that for all $h \in \mathcal{I}_H$:

- targets are perfectly located, with no ambiguity in range gates $l_{0,h}$, namely $\tau_{0,h} = l_{0,h} T_s$ with $l_{0,h} \in \mathcal{I}_L$;
- Doppler effects boil down to frequency shifts $F_{d,h} = 2v_h F_c/c$ such that $F_{d,h} \ll 1/T_s$, with F_c the carrier frequency of $\mathbf{s}$ and c the speed of light;

Assuming that clutter returns can be disregarded, the sampled baseband received radar signal is then

$$\mathbf{r} = \sum_{h=0}^{H-1} \alpha_h \mathbf{Z}_h \mathbf{s} + \mathbf{n} \tag{2}$$

where $[\mathbf{Z}_h]_{(l,l') \in \mathcal{I}_{ML} \times \mathcal{I}_{ML}} = e^{j2\pi f_{d,h} l/L} \delta_{l,l'+l_{0,h}}$ models the range-Doppler shifts induced by the hth target on $\mathbf{s}$, with $f_{d,h} = F_{d,h} L T_s$ its normalized Doppler frequency, and $\mathbf{n} \sim \mathcal{CN}(\mathbf{0}, \sigma^2 \mathbf{I}_{ML})$ denotes the white thermal noise vector.

3) Radar RX: The 3-stage low-complexity processing of [1] that assumes a range-Doppler tolerant waveform [2, Eq. (6)] is then performed on the received radar signal (2), namely: (i) linear symbol estimation; (ii) symbol removal; (iii) range-Doppler map computation. It is condensed into

$$\mathbf{x} = \underbrace{(\mathbf{F}_M \otimes \mathbf{F}_K^H)}_{\text{(iii)}} \underbrace{\mathbf{D}_{\mathbf{d}}^{-1}}_{\text{(ii)}} \underbrace{[\mathbf{I}_M \otimes (\mathbf{F}_K \mathbf{P}^T \mathbf{D}_{\check{\mathbf{g}}}^H)]}_{\text{(i)}} \mathbf{r} \tag{3}$$

with $\mathbf{D}_{\check{\mathbf{g}}} = \mathrm{diag}(\check{\mathbf{g}})$ where $\check{\mathbf{g}} = [\check{g}[0], \ldots, \check{g}[L-1]]^T$ is the receive pulse-shape vector with $\|\check{\mathbf{g}}\|^2$ determined by $\|\mathbf{g}\|^2$ and the waveform's PR condition, and $\mathbf{D}_{\mathbf{d}}^{-1} = \mathrm{diag}^{-1}(\mathbf{d})$. The presented system model is summed up in Fig. 2. In practice, note that zero-padding can be exploited in step (iii), subject to few changes in the expressions of (3).

C. Focus on the self-interference phenomenon

Let first consider the single-target case (*i.e.*, $H = 1$) and drop the index on the target parameters. Due to the time-frequency selective radar channel (2), the range-Doppler map $\mathbf{x}$ can be split into 3 terms [3]:

$$\mathbf{x} = \mathbf{x}^{(t)} + \mathbf{x}^{(i)} + \mathbf{x}^{(n)} \tag{4}$$

with $.^{(t)}$ and $.^{(n)}$ the resulting useful signal and noise, and $.^{(i)}$ the intercarrier-plus-interblock interference, or self-interference from a target detection perspective. Provided that $\mathbb{E}\{\alpha\} = 0$, it has been proved that [4]

$$\begin{aligned} \mathbb{E}\left\{ \mathbf{x}^{(t)^H} \mathbf{x}^{(t)} \right\} &= \sigma_t^2, \\ \mathbb{E}\left\{ \left(\mathbf{x}^{(n)} + \mathbf{x}^{(i)} \right) \left(\mathbf{x}^{(n)} + \mathbf{x}^{(i)} \right)^H \right\} &= \left(\sigma_n^2 + \sigma_i^2 \right) \mathbf{I}_{KM} \end{aligned} \tag{5}$$

where variances of the target σ_t^2, noise σ_n^2 and self-interference σ_i^2 detailed in (5a)-(5c) involve $\sigma_d^2 \triangleq \mathbb{E}\{|d_{k,m}|^2\}$, $\sigma_{d^{-1}}^2 \triangleq \mathbb{E}\{1/|d_{k,m}|^2\}$ as well as the cross-ambiguity function of $\check{g}$, g

$$A_{\check{g},g}(l,f) = K^{-1} \sum_{p=-\infty}^{+\infty} \check{g}[p] g[p-l] e^{j2\pi f p}.$$

In practice, (5) means that a highly reflective target (*i.e.*, $\mathbb{E}\{|\alpha|^2\} \gg 1$) induces a significant white self-interference-plus-noise level in the range-Doppler map which is emphasized as l_0 and/or f_d is high, namely as the loss on the target peak $|A_{\check{g},g}(l_0, f_d/L)|^2$ grows.

The latter phenomenon is all the more concerning as the number of targets H increases in (2). Indeed, if assuming statistical independence between targets, then by linearity of the radar processing (3) the self-interference power becomes

$$\sigma_i^2 = \sum_{h=0}^{H-1} \sigma_{i,h}^2 \tag{6}$$

with $\sigma_{i,h}^2$ the self-interference power related to target h and defined in (5c). As a result, the cumulated self-interference-plus-noise contribution is susceptible to mask weak targets in the range-Doppler map, as exemplified in Fig. 5a.

III. Successive self-interference cancellation

The CLEAN algorithm was originally introduced to fight sidelobes masking effects in radio astronomy [5], then in radar [6]. Herein we adapt this *ad-hoc* procedure to curb the aforementioned self-interference masking phenomenon while maintaining a low-complexity radar receiver processing. Performance and robustness analyses are provided.

$$\sigma_t^2 = \mathbb{E}\{|\alpha|^2\} KM \left| A_{\check{g},g}\left(l_0, \frac{f_d}{L}\right)\right|^2 \tag{5a}$$

$$\sigma_n^2 = \sigma^2 \sigma_{d-1}^2 K^{-1} \left\|\check{\mathbf{g}}\right\|^2 \tag{5b}$$

$$\sigma_i^2 \underset{M\gg 1}{\simeq} \mathbb{E}\{|\alpha|^2\} \sigma_d^2 \sigma_{d-1}^2 \left[\sum_{k=1}^{K-1} \left| A_{\check{g},g}\left(l_0, \frac{f_d}{L} + \frac{k}{K}\right)\right|^2 + \sum_{k=0}^{K-1} \left| A_{\check{g},g}\left(l_0 - L, \frac{f_d}{L} + \frac{k}{K}\right)\right|^2\right] \tag{5c}$$

A. Presentation of the procedure

The proposed SIC is described in Alg. 1. It takes the received signal (2) as an input. Then, at each iteration the procedure: computes a range-Doppler map following (3); detects the most powerful contribution in it ($|\cdot|$ denoting the elementwise modulus); deduce and store the corresponding range, Doppler and complex amplitude while compensating for the peak loss evidenced in (5a)[1]; update the received signal by removing the estimated contribution from it. The algorithm keeps running until a predefined stop criterion is met. As an output, it provides a clean range-Doppler map built synthetically from the stored parameters. Note that the procedure can be easily adapted to handle zero-padded versions of (iii) in (3) (as done in Section III-B2).

Algorithm 1 Proposed CLEAN-based procedure

Input: Received signal $\mathbf{r}$

Initialization: $j = 0$.

while the stop criterion is not met **do**

Compute $\mathbf{x}$ following (3).

Find $(\hat{k}_j, \hat{m}_j) = \text{argmax}_{(k,m)\in\mathcal{I}_K\times\mathcal{I}_M} [|\mathbf{x}|]_{k+mK}$.

Get $\hat{l}_{0,j} = \hat{k}_j$ and $\hat{f}_{d,j} = \hat{m}_j/M$.

Deduce $\hat{\mathbf{Z}}_j$ following (2) and compute $\hat{\alpha}_j = [\mathbf{x}]_{\hat{k}_j+\hat{m}_j K}/(\sqrt{KM} A_{\check{g},g}(\hat{l}_{0,j}, \hat{f}_{d,j}/L))$.

Update: $\mathbf{r} \leftarrow \mathbf{r} - \hat{\alpha}_j \hat{\mathbf{Z}}_j \mathbf{s}$ and $j \leftarrow j+1$.

end while

return Synthetic clean range-Doppler map estimate: $[\hat{\mathbf{x}}_{\text{clean}}]_{k+mK} = \sqrt{KM} \sum_{i=0}^{j-1} \hat{\alpha}_i \delta_{\hat{k}_i,k} \delta_{\hat{m}_i,m}$.

In the following simulations and unless otherwise specified, we assume that target amplitudes α_h are deterministic and that their number H is known in advance, so that the algorithm stops after H iterations. Also, in what follows, estimates $\widehat{\sigma_n^2 + \sigma_i^2}$ of the self-interference-plus-noise power are computed from all the range-Doppler bins that contain non-target contributions only.

B. Performance in a single-target scenario ($H = 1$)

1) On-grid: Herein we consider a single on-grid target with given range and Doppler frequency. We plot in Fig. 3 the normalized mean-squared error (NMSE) of our estimate $\hat{\alpha}$, defined as

$$\text{NMSE}(\hat{\alpha}) \triangleq \frac{\mathbb{E}\{|\alpha - \hat{\alpha}|^2\}}{\mathbb{E}\{|\alpha|^2\}} \tag{7}$$

[1]but not for the induced self-interference contribution in the cell.

for varying pulse-shapes and expansion factors L/K, as a function of the theoretical Signal-to-Noise-Ratio (SNR_{th}). The latter is achieved when the target is located in $(l_0, f_d) = (0, 0)$ and therefore does not induce any self-interference, namely [2]

$$\text{SNR}_{\text{th}} = \frac{\mathbb{E}\{|\alpha|^2\} K^2 M}{\sigma^2 \sigma_{d-1}^2 \left\|\check{\mathbf{g}}\right\|^2}. \tag{8}$$

In addition, and to avoid overloading the figure, we plot the normalized Cramér-Rao lower bound (NCRLB) of α for a single waveform setting (*i.e.*, CP-pulses with $L/K = 12/8$), derived from the signal model in the target range-Doppler cell when neglecting $x^{(i)}$, *i.e.*,

$$x = \alpha\sqrt{KM} A_{\check{g},g}(l_0, f_d/L) + x^{(n)} \tag{9}$$

where $x^{(n)} \sim \mathcal{CN}(0, \sigma_n^2)$. We observe that the NCRLB and the corresponding NMSE match in between two values of SNR_{th}, roughly 15 and 30 dB:

- below, the target peak in the range-Doppler map is insufficient to be reliably detected and estimated by the procedure;
- beyond, the target is very reflective and thus detected but $x^{(i)}$ is no longer negligible in the target bin (9). As SNR_{th} keeps growing, the NMSE even tends to a constant value.

These interval values actually depend on the target parameters (*i.e.*, the radar scene) together with the waveform parameters, as hinted by Fig. 3.

2) Robustness to off-grid: Now suppose that the target is not perfectly located in its range gate, *i.e.*, $l_0 = \lfloor l_0 \rfloor + \epsilon_{l_0}$ with $\lfloor\cdot\rfloor$ the floor function and $\epsilon_{l_0} \in [0, 1)$. Compared to (9), the target term incurs a straddle loss that may degrade our estimate of α and therefore the performance of the procedure. In Fig. 4 we quantify these degradations in terms of NMSE of $\hat{\alpha}$ and residual self-interference-plus-noise power measured in the updated range-Doppler map $\mathbf{x}$, respectively, both as a function of the misalignment ϵ_{l_0}. It is seen that zeropadding the initial range-Doppler map (in the range dimension) by a factor $zp_K = 4$ or $zp_K = 8$ leads to greatly lowered NMSE and more importantly, to an efficient self-interference removal. Similar conclusions are drawn regarding the Doppler dimension. The procedure is thus quite robust to off-grid provided that a sufficient zeropadding is performed beforehand, namely in stage (iii) of the radar receiver (3).

C. Performance in a multitarget scenario ($H > 1$)

Herein we consider the radar scene described in Table I containing $H = 3$ statistically independent on-grid targets and

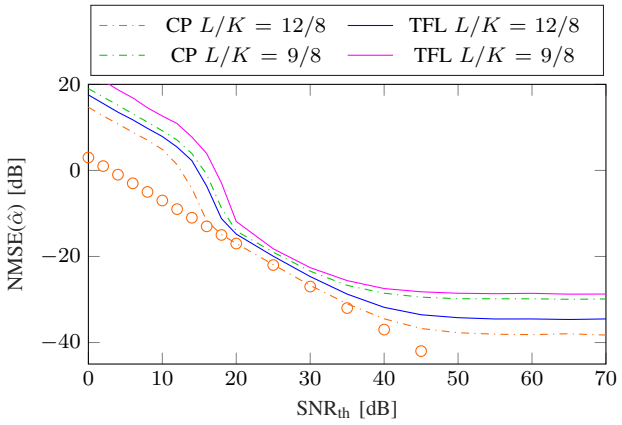

Fig. 3. NMSE of $\hat{\alpha}$ obtained with our CLEAN-inspired procedure as a function of the theoretical SNR. Monte-Carlo simulation on 3,000 runs. QPSK symbols such that $\sigma^2_{d^{-1}} = 1$, $K = 64$, $M = 32$, $\sigma^2 = 1$, varying L/K and pulses, target located in $(l_0, f_d/L) = (35, 1/(4K))$ and $\mathbb{E}\{|\alpha|^2\}$ defined by (8). Circle markers represent the NCRLB of α in model (9) for CP-pulses with $L/K = 12/8$.

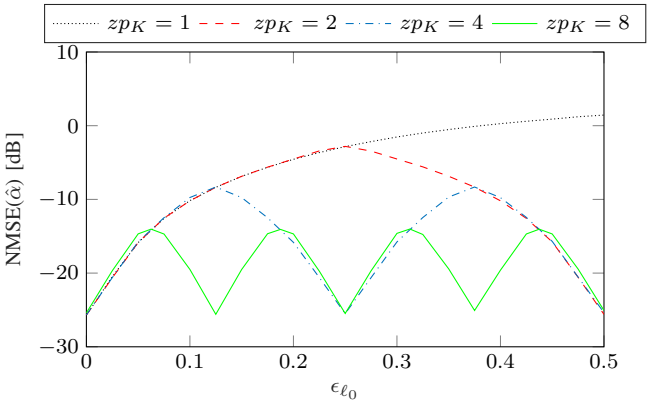

(a) NMSE of $\hat{\alpha}$ ($j = 0$ in Alg. 1)

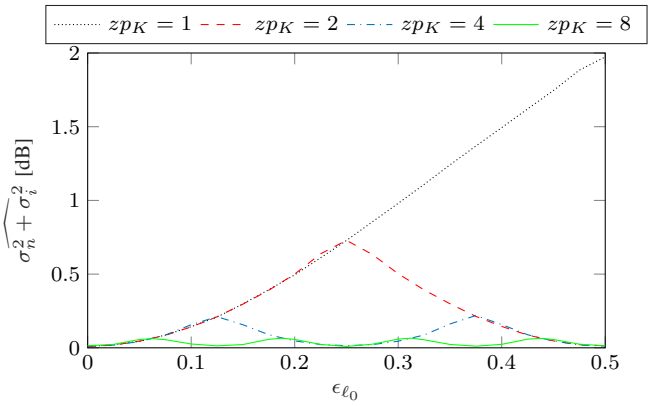

(b) Residual self-interference-plus-noise power ($j = 1$ in Alg. 1)

Fig. 4. Off-grid performance analysis of the proposed procedure for a varying zeropadding factor in range zp_K. Monte-Carlo simulation on 3,000 runs. QPSK symbols such that $\sigma^2_{d^{-1}} = 1$, $K = 64$, $M = 32$, $L/K = 12/8$, TFL-pulses, $\sigma^2 = 1$. SNR$_{\text{th}} = 35$ dB, the target is located in $(l_0, f_d/L) = (35 + \epsilon_{l_0}, 1/(4K))$ with $\epsilon_{l_0} \in [0, 0.5]$ and is correctly detected by the procedure. Initial self-interference-plus-noise power ($j = 0$ in Alg. 1): $\widehat{\sigma_n^2 + \sigma_i^2} = 3.02$ dB.

displayed in the range-Doppler domain in Fig. 5a when using CP-pulses with $L/K = 12/8$. In this scenario, the weakest target (*i.e.*, index $h = 2$) can hardly be distinguished from the self-interference-plus-noise level, mainly produced by the most powerful target $h = 0$ (namely, the one from Fig. 3). Alg. 1 is thus performed on the received signal $\mathbf{r}$, and results after 2 iterations are illustrated in the rest of Fig. 5. We notice that target $h = 2$ can then be easily detected and removed by the algorithm. This observation is confirmed in Fig. 6 (orange dashdotted curve) where the NMSE of $\hat{\mathbf{x}}_{\text{clean}}$

$$\text{NMSE}(\hat{\mathbf{x}}_{\text{clean}}) = \frac{\mathbb{E}\{\|\mathbf{x}_{\text{clean}} - \hat{\mathbf{x}}_{\text{clean}}\|^2\}}{\mathbb{E}\{\|\mathbf{x}_{\text{clean}}\|^2\}} \tag{10}$$

indeed reaches a minimum at iteration $j = 3$, $\mathbf{x}_{\text{clean}}$ being the clairvoyant clean range-Doppler map

$$[\mathbf{x}_{\text{clean}}]_{k+mK} = \sqrt{KM} \sum_{h=0}^{H-1} \alpha_h \delta_{(l_{0,h}),k} \delta_{(f_{d,h}M),m}.$$

While keeping the same radar scene, we now assume that the operator of the RadCom system uses another set of pulse-shapes and expansion factor, namely TFL-pulses with $L/K = 9/8$. The corresponding NMSE of $\hat{\mathbf{x}}_{\text{clean}}$ is depicted in Fig. 6 (magenta solid line). It is seen that having a higher self-interference power (as hinted by Fig. 3) might require more iterations of the SIC to achieve the NMSE minimum than the actual number of targets in the radar scene. In this specific setting, the procedure indeed often requires 2 iterations to completely extract the signature of target $h = 0$. However, this additional iteration is not necessarily detrimental given the low-computational complexity of the procedure. Plus, if it is to occur after having detected targets $h = 1$ and $h = 2$ (*i.e.*, once the procedure's purpose is already achieved) it may even be avoided with an appropriate stop criterion. The extra-cost may even be worth it here since it benefits to spectral efficiency.

TABLE I
TARGETS PARAMETERS FOR FIG. 6

h	0	1	2
$l_{0,h}$	35	10	20
$f_{d,h}/L$	$1/(4K)$	$1/(12K)$	$1/(6K)$
SNR$_{\text{th},h}$ (dB)	50	22	17

IV. Conclusion

In this paper, we implemented a CLEAN-based SIC procedure to iteratively remove the self-interference induced by targets throughout a previously described WCP-OFDM symbol-based radar processing. Particularly, we show that the proposed method may be an efficient way to overcome masking issues due to self-interference contributions, while keeping a low-complexity radar receiver. However, to that end, an appropriate stop criterion still needs to be defined to ensure an optimal estimation of the interference-free range-Doppler map while avoiding error propagation.

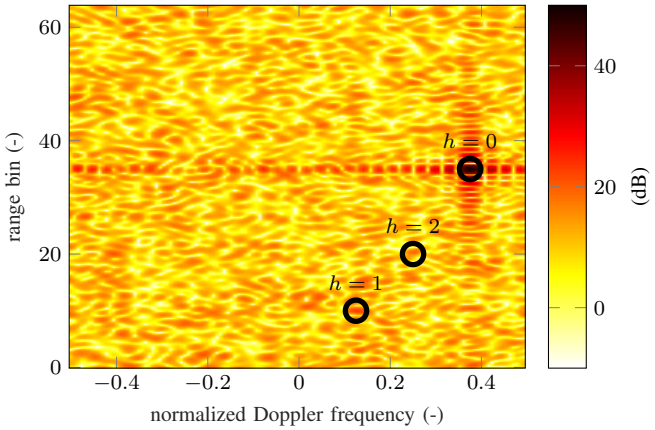

(a) Iteration $j = 0$ - $\widehat{\sigma_n^2 + \sigma_i^2} = 11.32$ dB

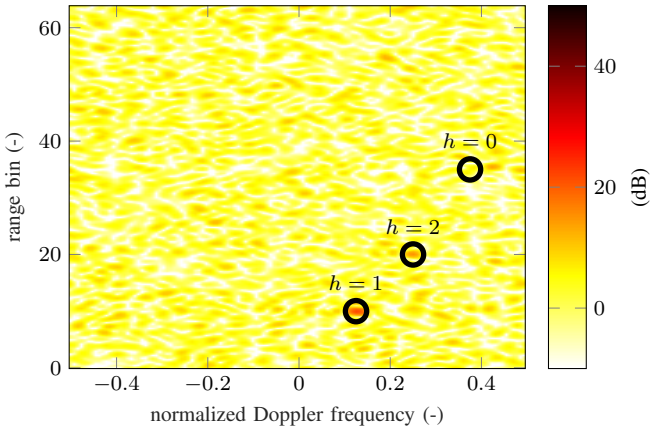

(b) Iteration $j = 1$ - $\widehat{\sigma_n^2 + \sigma_i^2} = 2.12$ dB

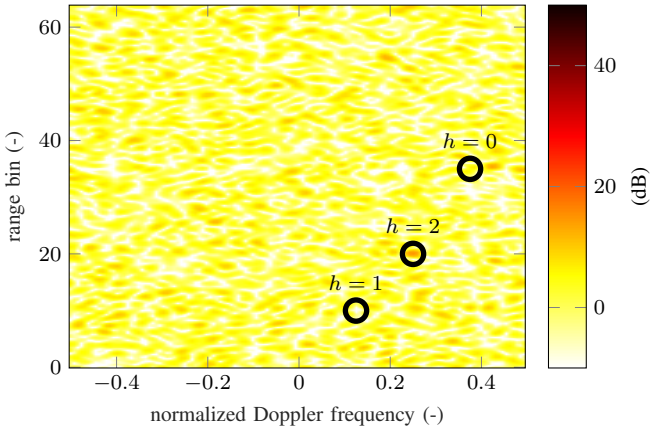

(c) Iteration $j = 2$ - $\widehat{\sigma_n^2 + \sigma_i^2} = 2.11$ dB

Fig. 5. Illustration of our CLEAN-based procedure on a range-Doppler map obtained from the radar scene in Table I. QPSK symbols such that $\sigma_{d-1}^2 = 1$, CP-pulses, $K = 64$, $M = 32$, $L/K = 12/8$, $\sigma^2 = 1$. Circles represent true targets locations. Detected peak $(\hat{l}_{0,j}, \hat{f}_{d,j}, |\hat{x}_j|^2)$ with $\hat{x}_j$ the measured amplitude in $(\hat{l}_{0,j}, \hat{f}_{d,j})$: (a) $(35, 0.375, 48.84$ dB); (b) $(10, 0.125, 21.02$ dB) and (c) $(20, 0.25, 14.58$ dB).

V. Acknowledgment

This work has been supported by DGA/MRIS under grant 2017.60.0005 and Thales DMS.

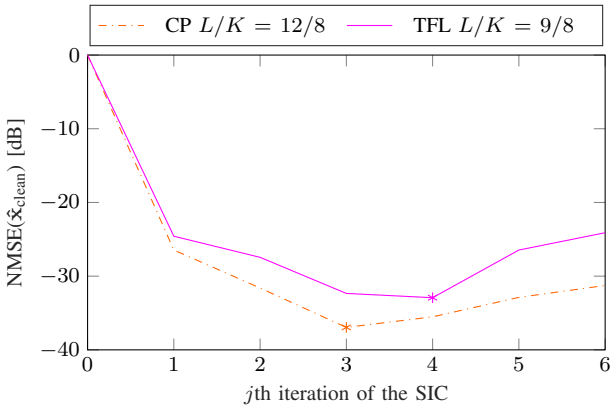

Fig. 6. NMSE of $\hat{\mathbf{x}}_{\text{clean}}$ as a function of the number of iterations of the SIC for the radar scene described in Table I. Monte-Carlo simulation on 5,000 runs. QPSK symbols such that $\sigma_{d-1}^2 = 1$, $K = 64$, $M = 32$, $\sigma^2 = 1$, varying pulses and expansion factors L/K. Asterisks used to indicate minimum values.

References

[1] C. Sturm, T. Zwick, and W. Wiesbeck, "An OFDM system concept for joint radar and communications operations," in *Veh. Tech. Conf., VTC Spring*, April 2009, pp. 1–5.

[2] D. Roque and S. Bidon, "Using WCP-OFDM signals with time-frequency localized pulses for radar sensing," in *Proc. IEEE Asilomar Conf. Signals, Syst. Comput.*, Nov. 2016, pp. 1154–1158.

[3] S. Mercier, S. Bidon, and D. Roque, "CA-CFAR detection based on an AWG interference model in a low-complexity WCP-OFDM receiver," in *Proc. IEEE Asilomar Conf. Signals, Syst. Comput.*, Oct 2017, pp. 1645–1649.

[4] S. Mercier, D. Roque, and S. Bidon, "Study of the target self-interference in a low-complexity OFDM-based radar receiver," *IEEE Trans. Aerosp. Electron. Syst.*, pp. 1–1, 2018.

[5] J. Högbom, "Aperture synthesis with a non-regular distribution of interferometer baselines," *Astronomy and Astrophysics Supplement Series*, vol. 15, p. 417, 1974.

[6] J. Tsao and B. D. Steinberg, "Reduction of sidelobe and speckle artifacts in microwave imaging: the CLEAN technique," *IEEE Trans. Antennas Propag.*, vol. 36, no. 4, pp. 543–556, Apr 1988.

[7] D. Pinchon and P. Siohan, "Closed-form expressions of optimal short PR FMT prototype filters," in *Proc. IEEE Global Telecommun. Conf. GLOBECOM*, 2011.

[8] Z. Wang and G. B. Giannakis, "Wireless multicarrier communications," *IEEE Signal Process. Mag.*, vol. 17, no. 3, pp. 29–48, May 2000.

[9] D. Roque and C. Siclet, "Performances of weighted cyclic prefix OFDM with low-complexity equalization," *IEEE Commun. Lett.*, vol. 17, no. 3, pp. 439–442, March 2013.